AIAA JOURNAL
Vol. 44, No. 8, August 2006

Interaction of Synthetic Jet Propulsion with Airfoil Aerodynamics at Low Reynolds Numbers

James Whitehead* and Ismet Gursul†
University of Bath, Bath, England BA2 7AY, United Kingdom

The use of synthetic (zero net mass flux) jets for the propulsion of fixed-wing small unmanned air vehicles was investigated. The formation of a time-averaged jet resulting from periodic excitation of a cavity and its interaction with separated flow over the airfoil were studied. As a thick trailing edge does not have an adverse effect on lift generation at low Reynolds numbers, a synthetic jet was placed at the trailing edge of the airfoil. It was shown that when the synthetic jet is activated the separated shear layer reattaches near the trailing edge of a cambered airfoil for momentum coefficients larger than a critical value, resulting in enhanced lift. For momentum coefficients larger than a critical value, the jet produces positive thrust, which strongly depends on excitation frequency. An optimum frequency range was identified, which produces maximum thrust. Aerodynamic efficiency was investigated as a function of the main parameters.

Nomenclature

A_E	=	aerodynamic efficiency
C_L	=	lift coefficient
C_p	=	pressure coefficient
C_T	=	thrust coefficient
C_μ	=	momentum coefficient
c	=	chord length
f	=	frequency
h	=	height of slot
p	=	pressure
p_∞	=	freestream pressure
Re	=	Reynolds number
Sr	=	Strouhal number
t	=	time
U_∞	=	freestream velocity
u	=	velocity in x direction
V	=	velocity magnitude
x	=	streamwise distance
y	=	cross-stream distance
α	=	angle of attack
ξ	=	vorticity
ρ	=	density

I. Introduction

RECENT interest in small unmanned air vehicles (UAVs) and micro air vehicles (MAVs) has been summarized in several review papers.[1–3] The aerodynamic and propulsion challenges associated with low-Reynolds-number flows in the range of $Re = 10^4$ to 10^5 pose a demanding engineering problem. Any vehicle on a truly microscale requires innovative and very recent technological solutions. A micro flying vehicle also has the additional considerations caused by relatively large weight and payload, small size and speed, and resulting low-Reynolds-number operation and poor efficiency. Continued advancement in microtechnology enhances the prospects of improving existing micro-air-vehicle concepts still further as well as presenting the possibility of new solutions. Although rotary and complex flapping wing designs have been successfully engineered and are useful for certain applications, recent work by Woods et al.[4] suggests that such methods of flight require considerably more energy than a fixed-wing vehicle in forward flight. This, together with the comparative simplicity of a fixed-wing vehicle, maintains interest in fixed-wing MAV research. However, there are significant aerodynamic and propulsion challenges associated with low-Reynolds-number flows.

It is well known that nearly all airfoil shapes show considerable sensitivity to the chord Reynolds number as it falls below10^5. Carmichael[5] showed that in the Reynolds-number range 10^4–10^5 airfoil performance also shows considerable sensitivity to changes in airfoil thickness. Completely separated flows are dominant in this low-Reynolds-number range. Thin airfoil sections appear to exhibit superior performance compared to airfoils above 6% thickness.[6–8] Laitone[6] showed that a thin wedge or thin cambered plate had higher lift coefficient than a NACA 0012 profile, as shown in Fig. 1 for $Re = 20.7 \times 10^3$. The performance of thin plates seems to be relatively insensitive to changes in Reynolds number and wind-tunnel turbulence. Laitone also showed that, when a NACA 0012 was reversed to use a sharp leading edge and blunt trailing edge, the lift coefficient was actually improved. Additional work[9] confirmed that in low-Reynolds-number aerodynamics lift is not as dependent on a sharp trailing edge as it is in higher-Reynolds-number flows. This suggests that the trailing-edge region could potentially be used for blowing or other flow-control purposes.

The conventional propulsion method for current micro air vehicles is propellers. Propeller efficiency drops very rapidly with decreasing Reynolds number for small MAVs. In addition, there is always some concern about the influence of propeller flow on MAV aerodynamics and control surfaces, as the propeller diameter approaches the size of the chord length of the wing. In this paper, the use of synthetic jets for the propulsion of fixed-wing MAVs is investigated as a possible alternative to propellers. Placement of a synthetic jet at the trailing edge[10,11] would seem sensible as a thick trailing edge appears not to have an adverse effect on the lift generation of MAVs.

A time-averaged jet resulting from periodic excitation of a cavity using a diaphragm is a phenomenon that has been known[12] since at least 1950. In the past 10 years or so, unsteady forcing techniques have been increasingly employed in flow-control applications, albeit under different names: oscillatory control,[13] internal acoustic excitation,[14] unsteady bleed technique,[15,16] and synthetic jets[17–24] as they are referred to here. The use of synthetic jets as flow control or flow reattachment devices is increasingly studied for medium- to high-Reynolds-number flows. Little work has been conducted using synthetic jets for low-Reynolds-number flows. In fact the small scale and weight of an MAV enables synthetic jets to be tried not

Received 23 June 2005; revision received 31 December 2005; accepted for publication 31 December 2005.

*Graduate Student, Department of Mechanical Engineering.
†Professor, Department of Mechanical Engineering. Associate Fellow AIAA.

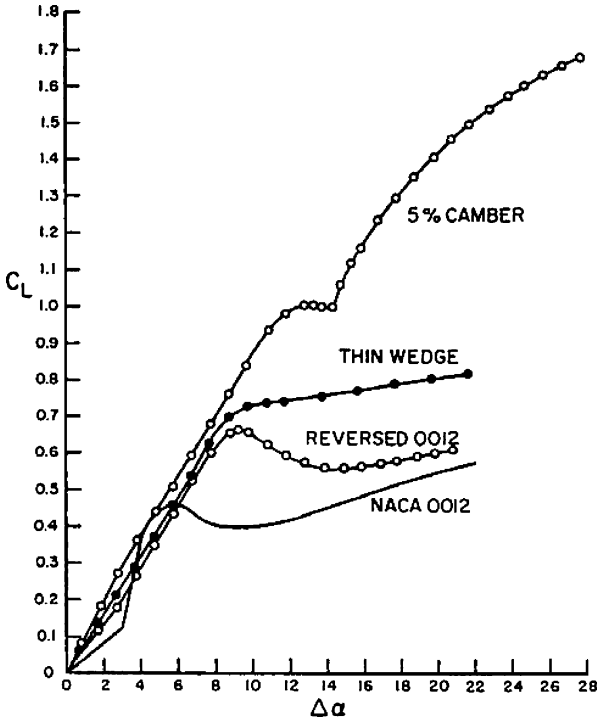

Fig. 1 Variation of lift coefficient with angle of attack for various airfoils.[6]

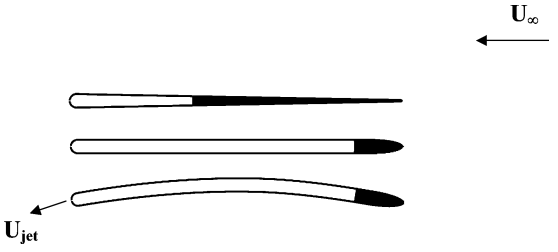

Fig. 2 Schematic of hollow airfoils studied.

only as a separation control device, but also as a propulsion device. Properties such as zero net mass flux, no external fluid and piping requiurements, and small size lend synthetic jets well to MAV technology.

The principal aim of this investigation is to explore and determine parameters for the use of synthetic jets as a solution to MAV propulsion and enhanced aerodynamics. Interaction of a synthetic jet located at the trailing edge with the low-Reynolds-number flow around the wing was investigated with flow visualization, velocity, and pressure measurements. In both wind-tunnel and water-tunnel experiments, particle image velocimetry (PIV), laser Doppler velocimetry (LDV), and pressure measurements were combined to understand the effects of excitation frequency, momentum coefficient, and angle of attack over the low-Reynolds-number regime.

II. Experimental Setup

Several hollow airfoils, with cross sections as shown in Fig. 2, were tested in the initial experiments.[10] All airfoils were constructed with 200-mm span and chord, and a 0.5 mm high 1 mm long (in the direction of the jet axis) slot at the trailing edge across the entire span. The first model tested was a thin wedge shape with a rounded trailing edge as shown at the top of Fig. 2. The leading edge and trailing edge had a thickness of 2 and 8 mm (corresponding to 1 and 4% thickness), respectively. For ease of modeling, both the leading edge and trailing edge were chosen to be semicircular in cross section with diameter equal to the local thickness. Two other models with the same chord length and trailing-edge geometry were

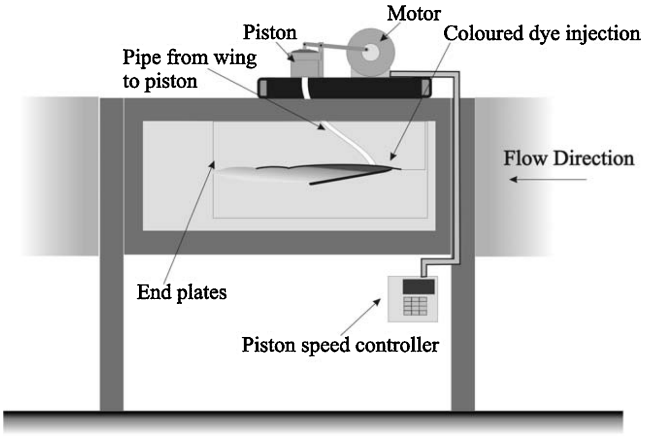

Fig. 3 Schematic of water-tunnel setup.

manufactured: one flat with 4% constant thickness and an elliptical leading edge (4:1 ratio), and the other identical but with a 5% camber as shown in Fig. 2. Initial flow visualization[10] suggested that the cambered airfoil had the best potential, which is consistent with previous work.[6,7,25]

Flow visualization was conducted in a free surface Eidetics water tunnel, with test section of dimensions 381×508 mm, located at the University of Bath. Models were placed between end plates for a quasi-two-dimensional simulation in these experiments. Hollow wings were connected with piping to a piston-cylinder arrangement located outside the test section as shown in Fig. 3. The synthetic jet was constructed from a water-tight stretchable rubber diaphragm oscillated using a mechanical armature and an electric motor. A variable speed controller for the motor allowed the jet excitation frequency to be varied, and a change in the piston armature could vary the jet amplitude. Initial flow-visualization experiments were conducted using this setup in the water tunnel at speeds of 5 to 15 cm/s, equivalent to chord Reynolds numbers of 10^4–3×10^4. Flow visualization was conducted by injecting food-coloring dye at different locations of the wing.

Further experiments were conducted in air, using a speaker to generate the synthetic jet as shown in Fig. 4a. The setup was placed in the open-section wind tunnel with a diameter of 76 cm at the University of Bath, as shown in Fig. 4b. The speaker could then be controlled using a signal generator, giving frequency and amplitude adjustments. Experiments were conducted in the Reynolds-number range of $Re = 10^4$ to 2×10^5, although the majority were under $Re = 6 \times 10^4$. Wind-tunnel turbulence intensity was around 0.4% for the smallest Reynolds number $Re = 10^4$ and around 0.3% for higher Reynolds numbers. Although certain airfoils (with relatively thick cross sections) show great sensitivity to freestream turbulence, which affects transition and separation bubbles at low Reynolds numbers, Laitone[9] reported that thin plates were relatively insensitive to the turbulence level for Reynolds numbers below 7×10^4.

The velocity measurements were conducted using a TSI PIV system, consisting of 120-mJ dual Nd:Yag lasers and a 4.2-MPixel digital camera, operating in cross-correlation mode at 7.5 Hz. The midspan plane was illuminated using a laser mirror as shown in Fig. 4b. A combination of cylindrical and spherical lenses was used to generate the laser light sheet. A TSI six-jet oil particle atomizer was used to generate seeding particles (around 1-μm diam) for both PIV and LDV measurements. PIV images were captured in a region near the trailing edge of the wing to study the separated region as well as the dynamics of the synthetic jet. A cross-correlation technique based on the fast-Fourier-transform algorithm was used to determine the velocity field. The interrogation window size was varied from 16×16 to 32×32 pixels with 50% overlap. The size of the area interrogated also varied depending on the region of interest, and the smallest area was approximately $0.15c \times 0.15c$. The effective grid size was varied between 0.34×0.34 and 1.25×1.25 mm, depending on the size of

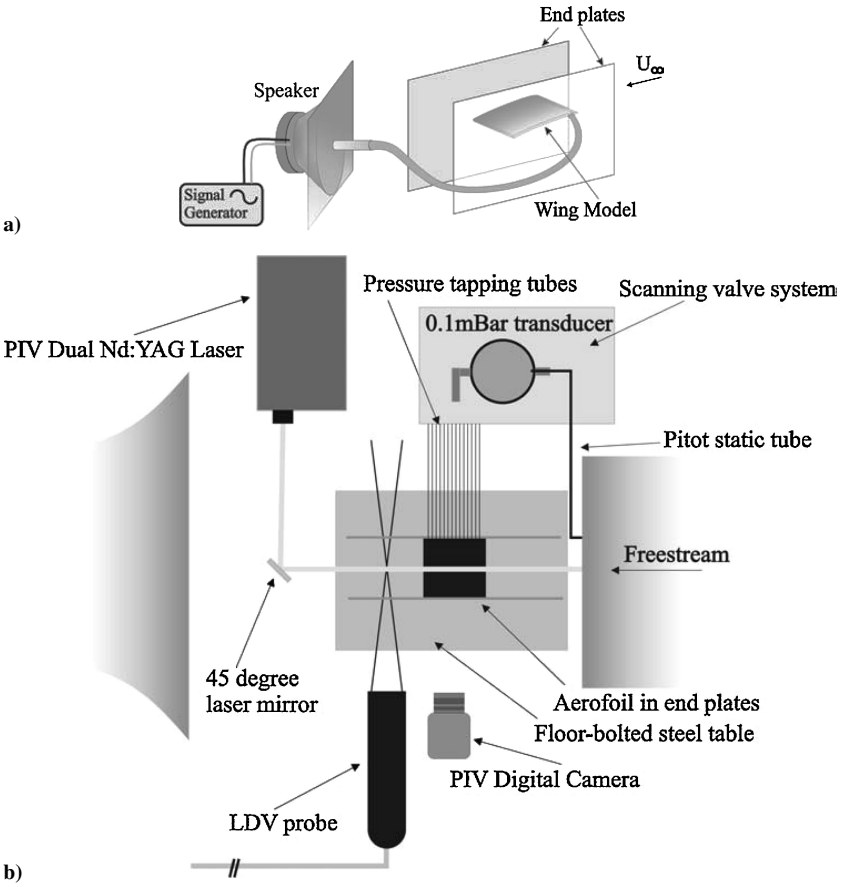

Fig. 4 Schematic of a) loudspeaker arrangement to generate synthetic jet in wind-tunnel experiments and b) wind-tunnel setup and measurement methods used in the open-section wind tunnel.

the region imaged. Sequences of 100 pictures were captured and averaged to obtain the time-averaged velocity field. Phase-locked measurements were obtained by using the external trigger of the PIV system connected to the synthetic jet driving signal. Sequences of 50 phase-locked PIV results were used to calculate representative phase-averaged measurements.

A two-component LDV system with 300-mW, air-cooled argon-ion laser was used to measure instantaneous velocity near the jet exit at the trailing-edge region to calculate the momentum coefficient C_μ in the absence of freestream. These measurements were taken at 1 mm downstream of the jet orifice ($x/h = 2$), and the measurement volume diameter was 65 μm. The data rate in air was of the order of a few thousand hertz, providing high time resolution for time-dependent velocity measurements. The momentum coefficient C_μ was calculated as

$$C_\mu = \frac{\rho \int_{-\infty}^{\infty} u^2 \, \mathrm{d}y}{\frac{1}{2}\rho U_\infty^2 c}$$

The estimated uncertainty for momentum coefficient was around 4%. The LDV system was also used to survey the velocity profiles in the wake. The overhead layout of the PIV, LDV, and pressure measurement apparatus in the open-section wind tunnel is shown in Fig. 4b.

Two high-sensitivity (0.1 and 1 mbar) differential pressure transducers were used to measure surface-pressure coefficients on a identical cambered airfoil, which was specially built for pressure measurements, in the range of $Re = 2 \times 10^4$ to 10^5. The cambered airfoil had 47 pressure tappings of 0.5-mm diam, distributed over the upper and lower airfoil surfaces.[26] The transducer was connected to a computer-controlled scanning pressure measurement system capturing at 1 kHz for each measurement location. The estimated uncertainty for pressure measurements was less than 4%. The mean

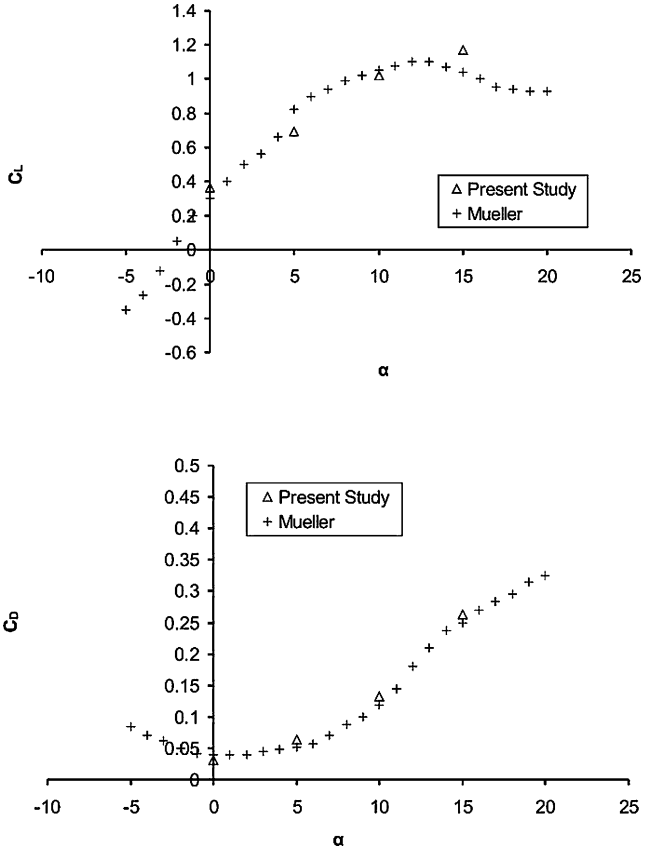

Fig. 5 Comparison of data from the present study with that of Mueller[7] for a similar airfoil at $Re = 6 \times 10^4$ without jet excitation.

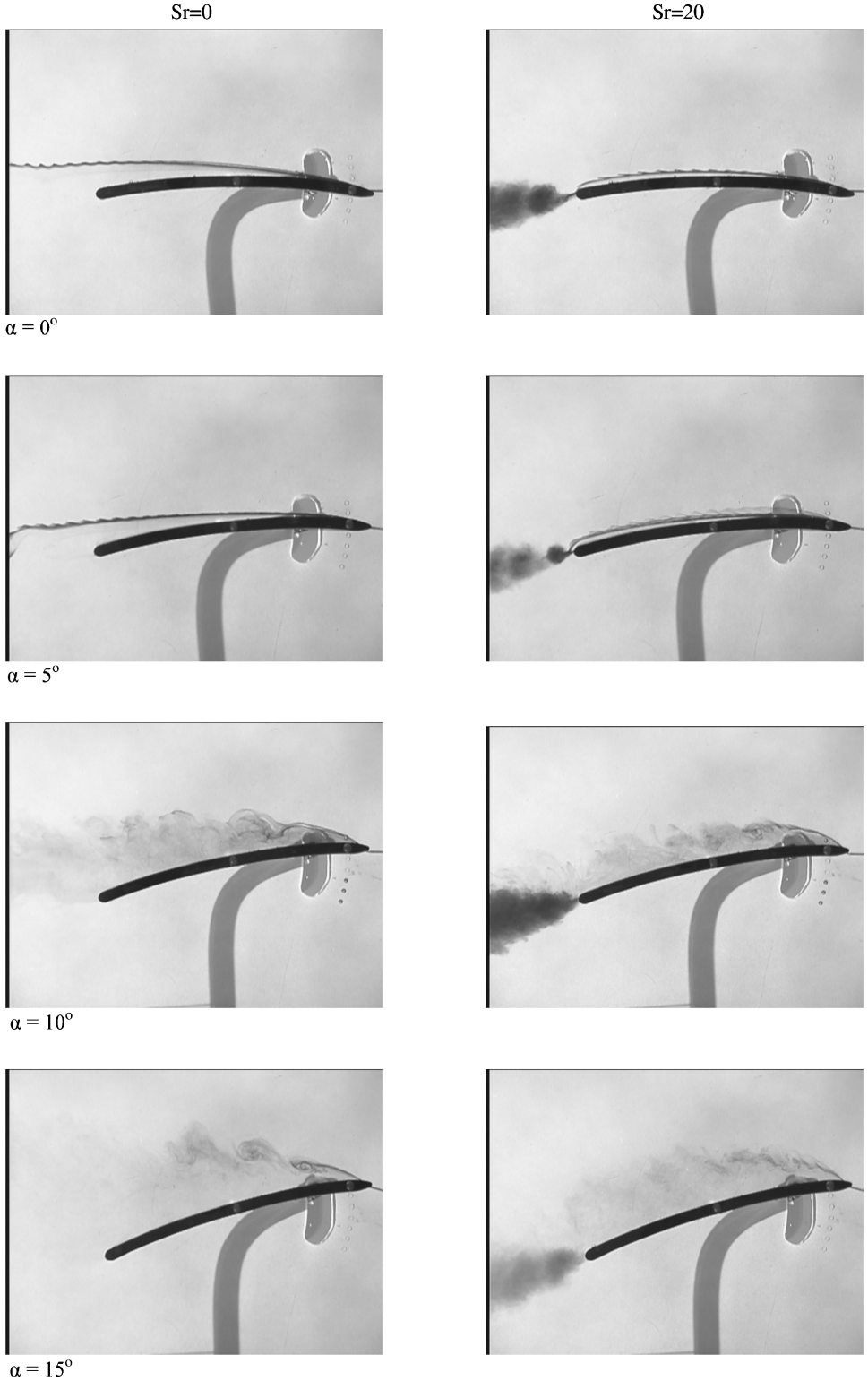

Fig. 6 Flow visualization pictures of cambered airfoil with and without synthetic jet at $Re = 10^4$.

surface-pressure coefficients were then calculated and used to estimate the lift and drag coefficients using the standard surface integral technique. The uncertainty for lift and drag was estimated to be 5%. Figure 5 shows a comparison between measurements conducted by Mueller[7] on a similar airfoil (but with a sharp trailing edge) to that of the present study without jet excitation. Good agreement is found between the data for both drag and lift coefficients.

The excitation frequency was made dimensionless by defining the Strouhal number as

$$Sr = fc/U_\infty$$

This dimensionless frequency based on the chord length was considered to be more appropriate than one based on the slot height,[21,27]

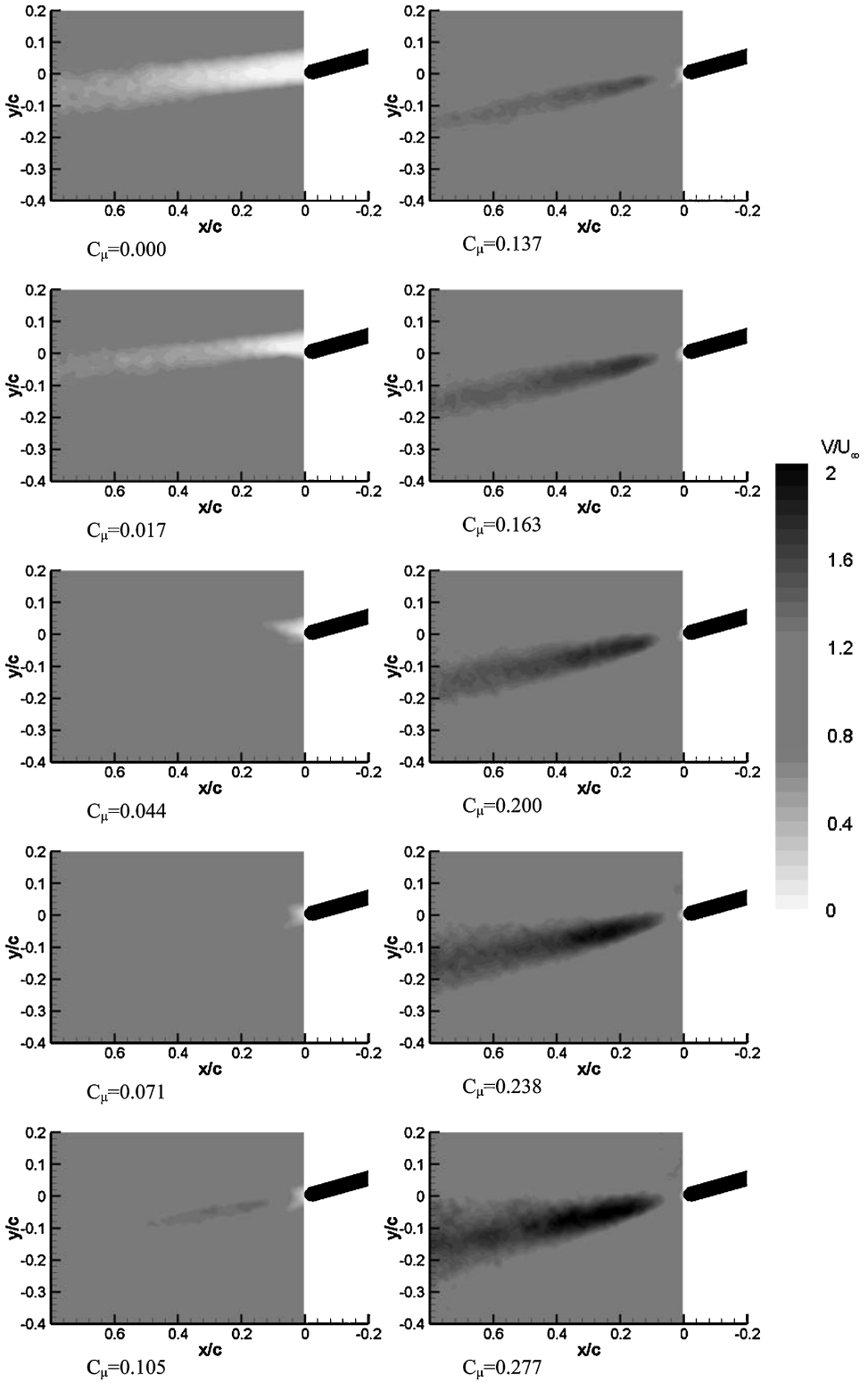

Fig. 7 Magnitude of time-averaged velocity for $Re = 10^4$, $\alpha = 5$ deg, and $Sr = 5.7$.

as the interaction of external aerodynamics with a synthetic jet is studied here. A modified version of the lift-to-drag ratio, termed aerodynamic efficiency A_E, was used to account for momentum injection, similar to that used by Seifert et al.[28]:

$$A_E = C_L/(C_\mu - C_T)$$

Without jet excitation, $C_\mu = 0$, and $C_T = -C_D$; therefore, $A_E = C_L/C_D$.

III. Results

A. Overview

Figure 6 shows an example of flow visualization from water-tunnel experiments without jet excitation, at $Sr = 0$, and with jet excitation at $Sr = 20$. At $Sr = 0$, injection of dye upstream of the leading edge shows that at low incidence at $Re = 10^4$, there is a laminar separated shear layer, originating from the airfoil surface slightly downstream of the leading edge. At higher incidences, the separated laminar region originates from the leading edge but loses coherence early over the airfoil and becomes turbulent.

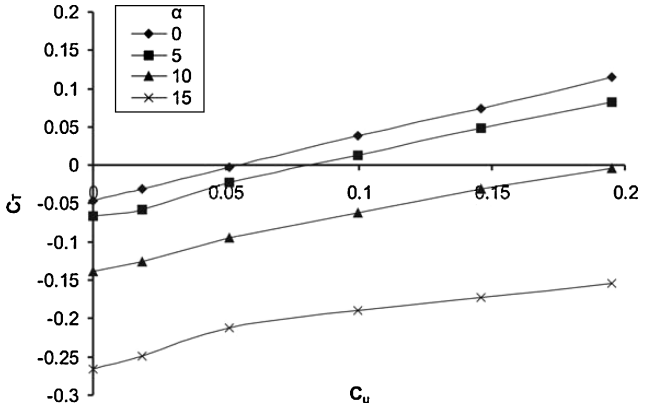

Fig. 8 Variation of estimated thrust coefficient with blowing coefficient C_μ at $Re = 2 \times 10^4$, $Sr = 2.9$.

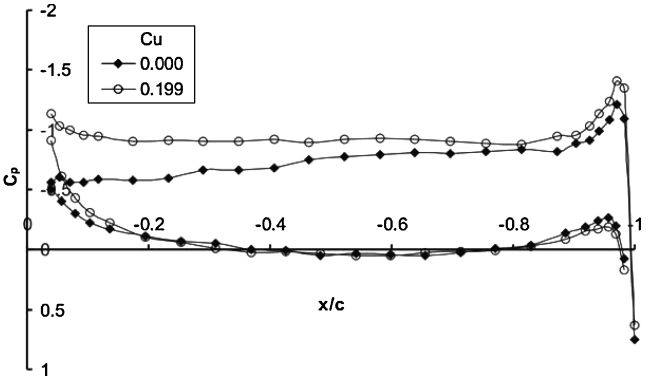

Fig. 9 Surface-pressure distribution for $Sr = 2.9$ and for no blowing at $Re = 4 \times 10^4$, $\alpha = 5$ deg.

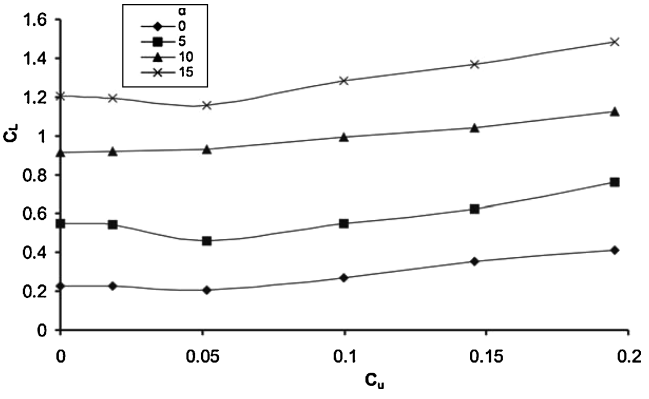

Fig. 10 Variation of estimated lift coefficient with blowing coefficient C_μ at $Re = 2 \times 10^4$, $Sr = 2.9$.

At all four incidences shown in Fig. 6, the effect of jet excitation at $Sr = 20$ is visualized by the injection of dye near the leading edge and also in the cavity of the airfoil. As the synthetic jet is formed at the trailing edge, the dye injection at the leading edge shows the flow reattachment over the upper surface at low angles of attack ($\alpha = 0$ and 5 deg). When the synthetic jet is activated, the separated shear layer reattaches near the trailing edge for the cambered wing, whereas this was not observed for the other two airfoils.[10] Therefore, the detailed experiments were conducted for the cambered airfoil only. At higher angles of attack ($\alpha = 10$ and 15 deg), the large flow separation region seen over the airfoil surface at $Sr = 0$ is greatly reduced with jet excitation at $Sr = 20$. The addition of the jet would therefore suggest not only a propulsive mechanism, but also a lift-enhancing device as a secondary benefit. In particular, at low angles of attack, the reattachment of the upper-surface flowfield suggests

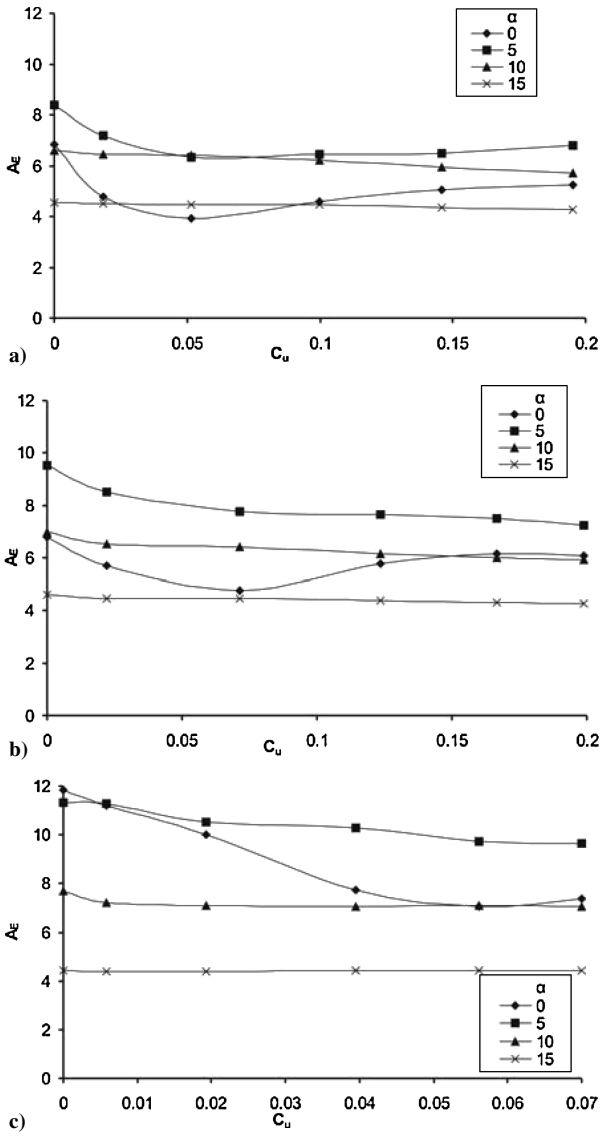

Fig. 11 Variation of aerodynamic efficiency with blowing coefficient C_μ at a) $Re = 2 \times 10^4$, b) $Re = 4 \times 10^4$, and c) $Re = 6 \times 10^4$, with $Sr = 2.9$.

enhanced lift during the synthetic jet operation. Detailed investigations of the effects of the momentum coefficient, frequency, angle of attack, and Reynolds number were made for the cambered airfoil. These effects are summarized next. In addition, development of an airfoil with internal actuation is described.

B. Effect of Momentum Coefficient

Figure 7 shows the effect of increasing the momentum coefficient on the time-averaged flow in the wake at $Re = 2 \times 10^4$ with $\alpha = 5$ deg and $Sr = 5.7$. The magnitude of the velocity shows the drag-indicative low-velocity region in the wake for $C_\mu = 0$. As the momentum coefficient is increased, the low-velocity region in the airfoil wake is reduced. For $C_\mu = 0.044$ and 0.071, the low-velocity region in the wake becomes comparatively small. Hence, when the momentum coefficient is near a critical value, zero net drag is produced, corresponding to a cruise condition for the MAV. Increasing the momentum coefficient above the critical value produces a jet-like profile in the wake and positive thrust. As Fig. 7 shows, increasing the momentum coefficient to higher values produces a jet with increasing strength, with larger jet width and larger time-averaged velocity in the wake. Maximum time-averaged jet velocities in the order of twice the freestream velocity are observed a short distance from the trailing edge.

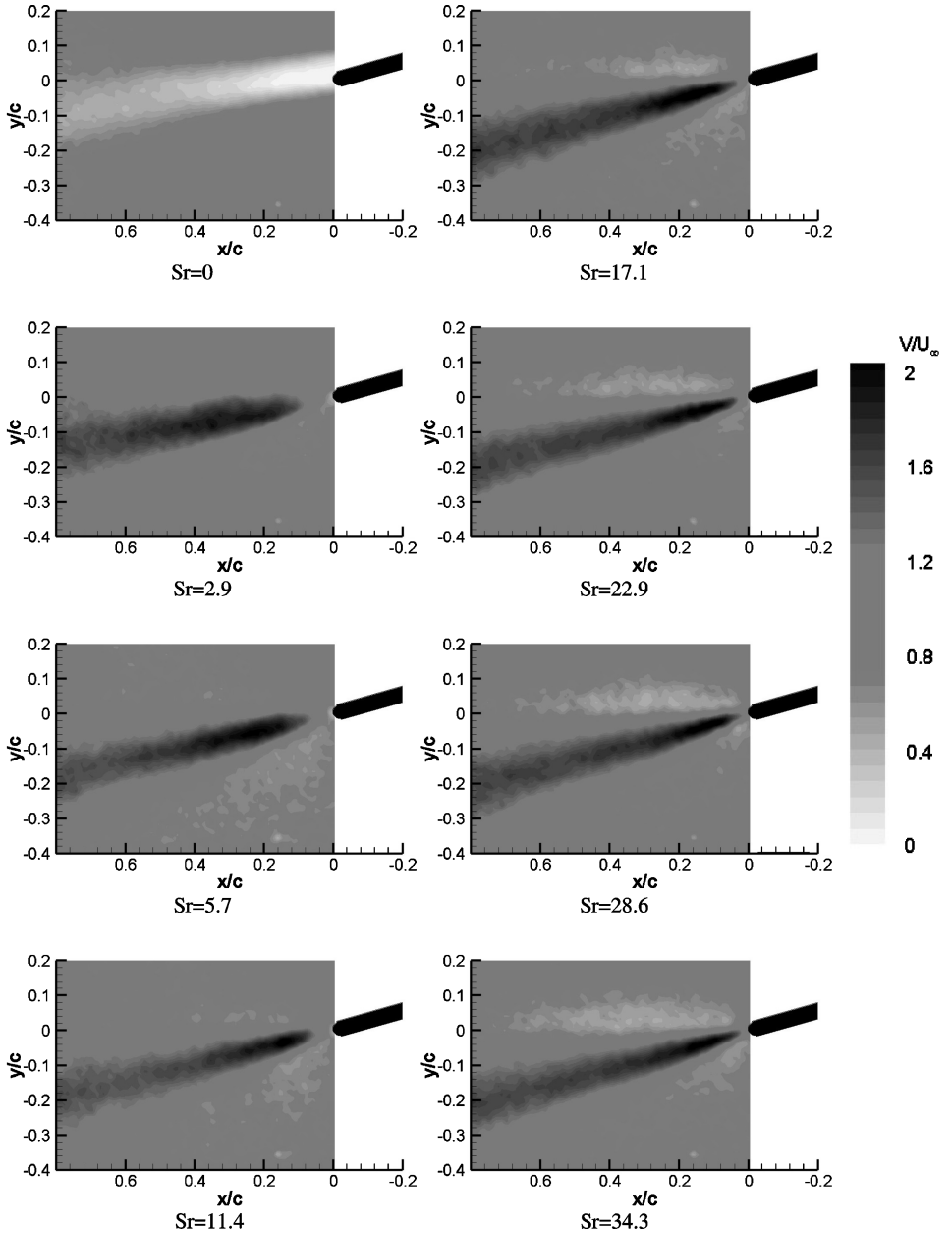

Fig. 12 Magnitude of time-averaged velocity for $Re = 10^4$, $\alpha = 5$ deg, and $C_\mu = 0.30$.

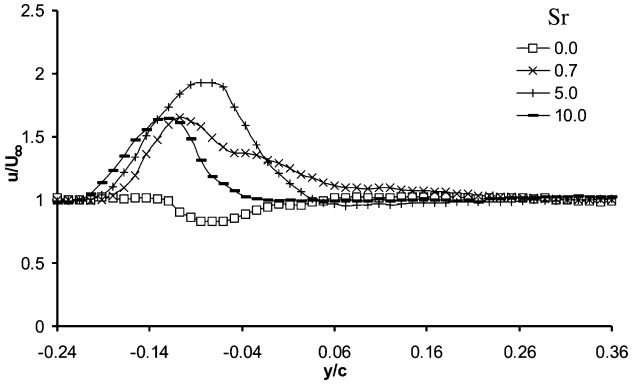

Fig. 13 Variation of time-averaged streamwise velocity profiles in the wake ($x/c = 0.5$) with frequency for $Re = 2 \times 10^4$, $\alpha = 5$ deg, and $C_\mu = 0.29$.

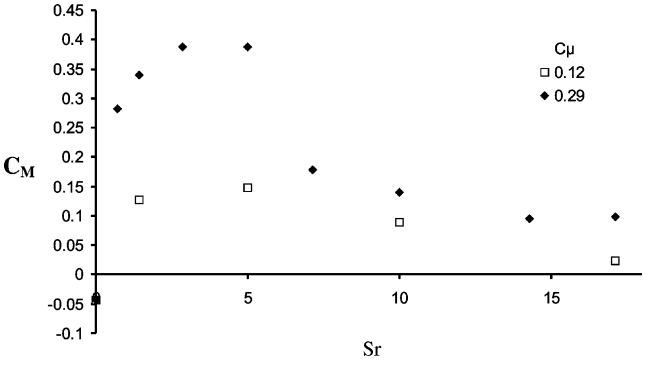

Fig. 14 Variation of momentum flux coefficient as a function of Strouhal number for $Re = 2 \times 10^4$, $\alpha = 5$ deg.

Figure 8 shows the variation of estimated thrust coefficient from pressure measurements as a function of momentum coefficient for various angles of attack and $Re = 2 \times 10^4$, $Sr = 2.9$. It is seen that at low incidences ($\alpha = 0$ and 5 deg), the critical momentum coefficient is between 0.05 and 0.07, whereas for larger incidences the net thrust is always negative in the range tested. However, the critical momentum coefficient depends on frequency and Reynolds number as will be discussed later on. For $\alpha = 10$ deg, almost zero net drag is obtained for the largest momentum coefficient. MAVs with low-aspect-ratio wings fly at high angles of attack to generate vortex lift, which might be a limiting factor for the present method. With the exception of the largest angle of attack $\alpha = 15$ deg, the trend of the thrust coefficient is linear with the momentum coefficient.

C. Lift Enhancement

Flow visualization shown in Fig. 6 suggested that shear-layer reattachment near the trailing edge was possible for sufficiently large momentum coefficient. To explore potential lift enhancement, detailed measurements of the time-avereged pressure[26] on the airfoil surface were made as a function of momentum coefficient for various frequencies and angles of attack in the range of $Re = 2 \times 10^4$ to 6×10^4. An example is shown in Fig. 9 for $Re = 4 \times 10^4$, $\alpha = 5$ deg, $Sr = 2.9$, and $Sr = 0$. It is seen that the upper-surface pressure distribution is significantly altered when the synthetic jet is activated for $C_\mu = 0.199$. Although the lower surface-pressure distribution is little affected, the upper surface pressure becomes more negative, in particular in the downstream half, as the pressure near the trailing

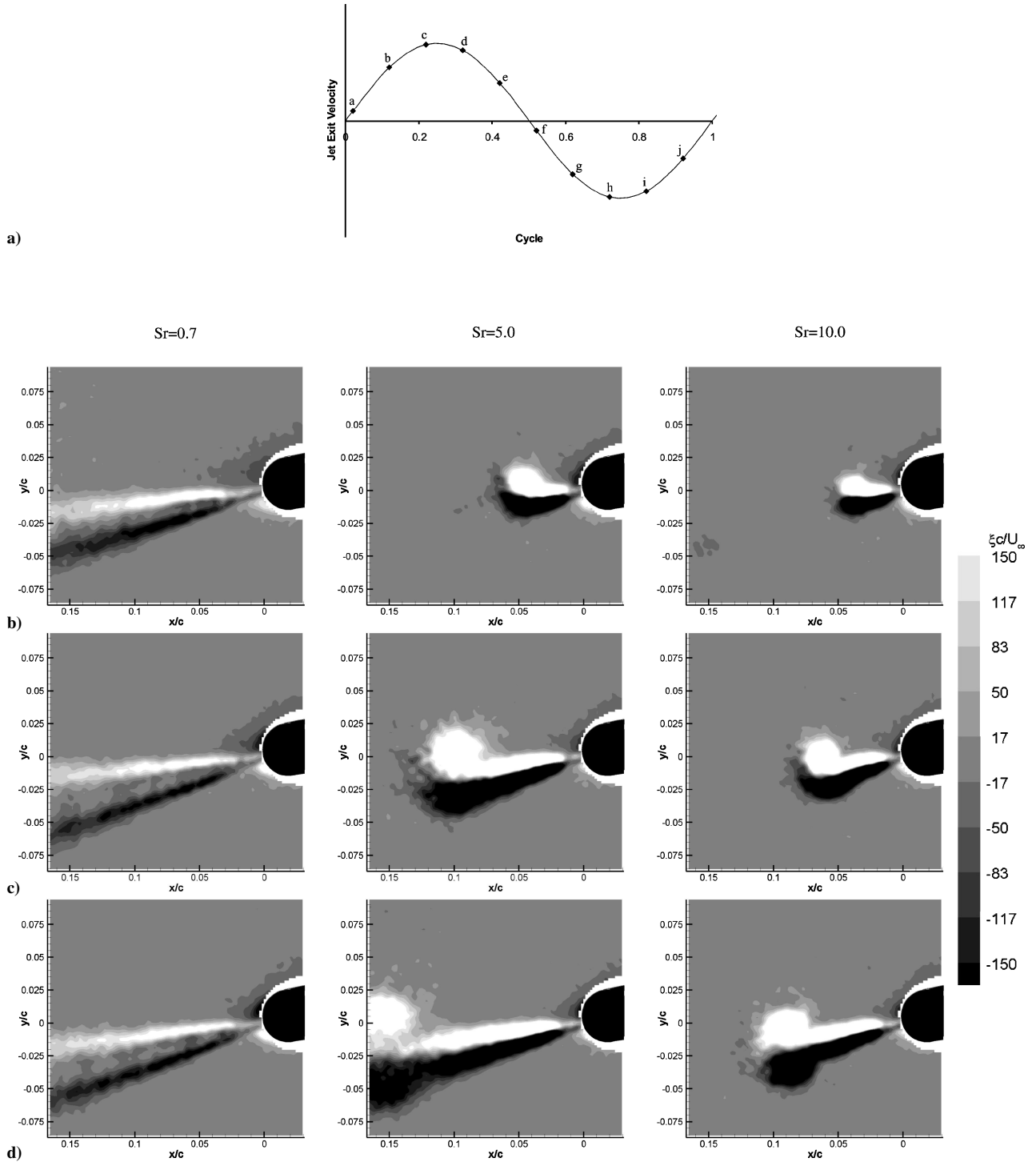

Fig. 15 Phase-averaged vorticity for three Strouhal numbers for $Re = 2 \times 10^4$, $\alpha = 5$ deg, and $C_\mu = 0.29$. Instants in the cycle are shown in panel a. Panels b–h correspond to phases b–h.

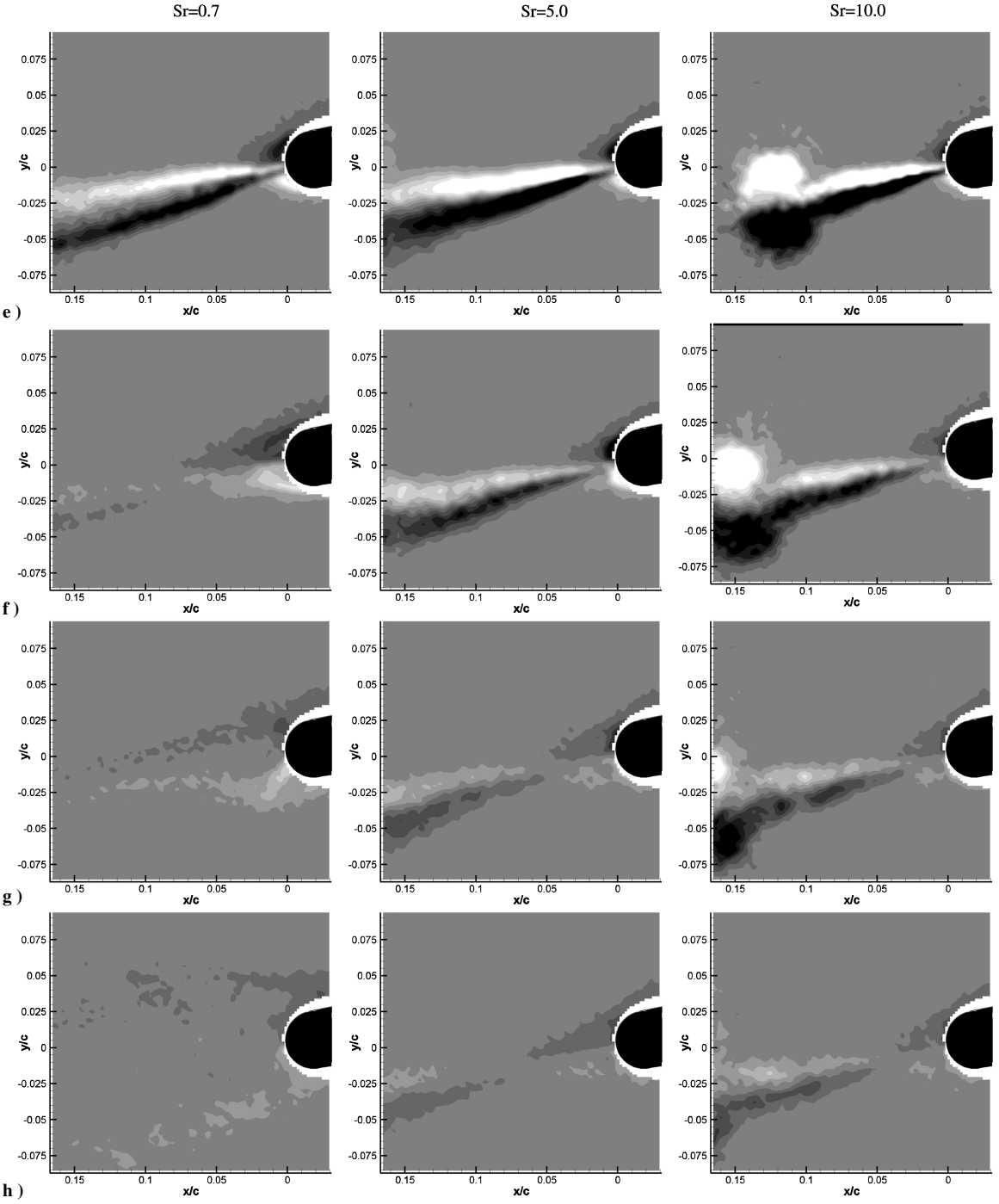

Fig. 15 Phase-averaged vorticity for three Strouhal numbers for $Re = 2 \times 10^4$, $\alpha = 5$ deg, and $C_\mu = 0.29$. Instants in the cycle are shown in panel a. Panels b–h correspond to phases b–h (continued).

edge drops from $Cp \cong -0.5$ to -1.2. This confirms the anticipated lift enhancement when the synthetic jet is activated.

The lift coefficient was estimated from these pressure measurements. Detailed results are given in Ref. 26. An example is given in Fig. 10, which shows the variation of lift coefficient with momentum coefficient for various angles of attack and $Re = 2 \times 10^4$, $Sr = 2.9$. It is seen that there is a slight decrease in lift at around the critical momentum coefficient, followed by a gradual increase in lift with further increase of momentum coefficient. The reason for the slight decrease for low momentum coefficients is not clear; however, the lift appears to increase linearly after this small decrease.

Assessment of the overall aerodynamic performance, accounting for the momentum injection and the resultant effects on both lift and thrust coefficient, is done by considering the aerodynamic efficiency A_E defined earlier. Figure 11 shows the variation of the aerodynamic efficiency as a function of momentum coefficient for Reynolds numbers $Re = 2 \times 10^4$, 4×10^4, and 6×10^4, for various angles of attack. The maximum momentum coefficient for the $Re = 6 \times 10^4$ case was $C_\mu = 0.07$ because of the limitations of the driving mechanism. It is seen that there is initially a decrease in the efficiency with increasing momentum coefficient for low angles of attack, but the efficiency is less affected at high angles of attack as the flow reattachment is not achieved. Although there is a slight decrease in aerodynamic efficiency with blowing at low angles of attack, this should not be considered as a disadvantage because the blowing is not used only as a flow-control (lift enhancement) device in this case. The main function of blowing is to provide thrust, and this also improves lift as a secondary benefit. The aerodynamic efficiency generally improves with increasing Reynolds number for low angles of attack, but again there is no change at higher angles of

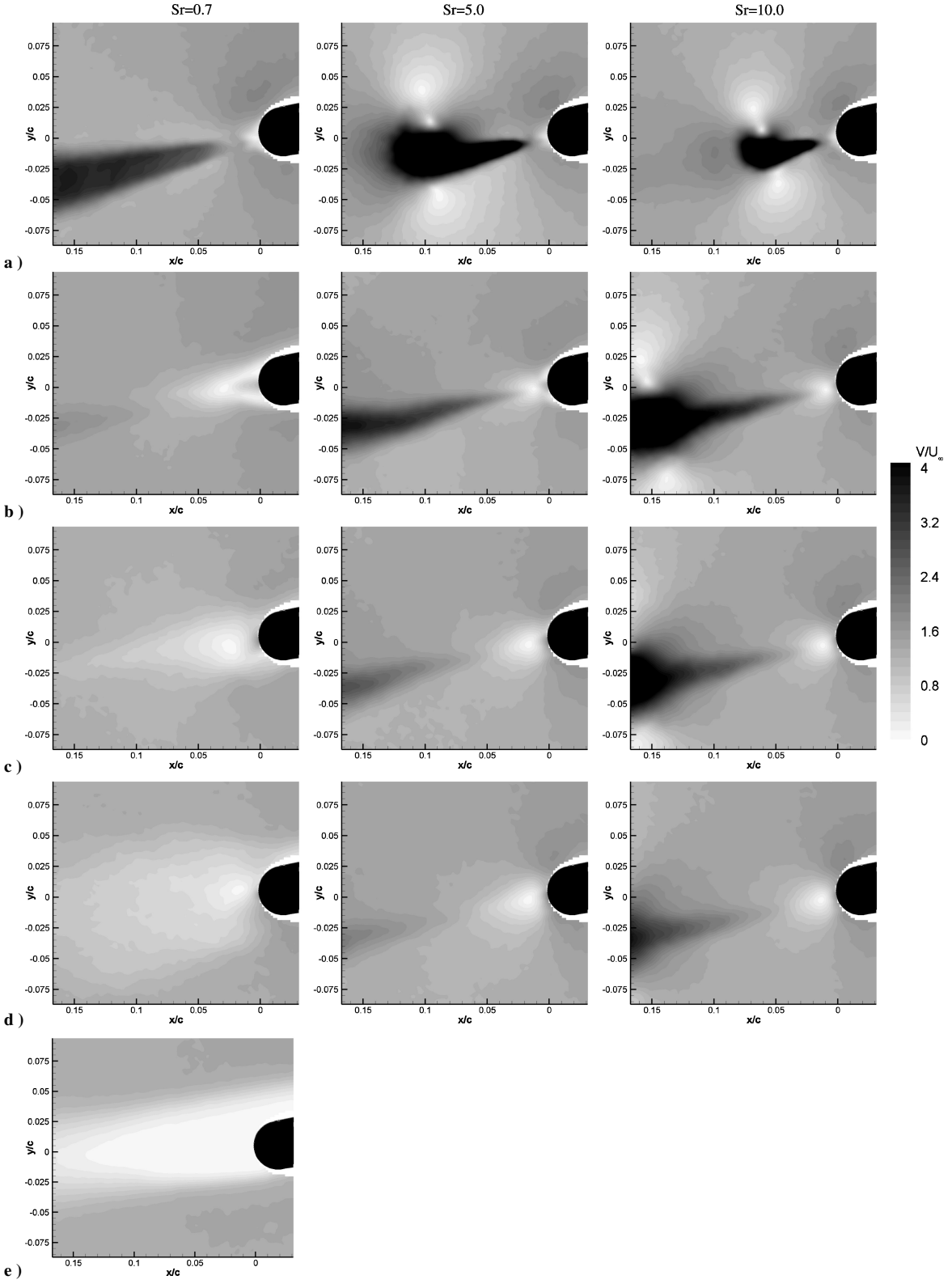

Fig. 16 Magnitude of phase-averaged velocity for three Strouhal numbers at instants indicated: $Re = 2 \times 10^4$, $\alpha = 5$ deg, and $C_\mu = 0.29$. Panels a, b, c, and d correspond to phases c, f, g, and h, respectively. Case for no blowing is shown in panel e for comparison.

attack. The maximum efficiency is observed for $\alpha = 5$ deg. Without excitation the aerodynamic efficiency (lift-to-drag ratio in this case) is shown to increase with Reynolds number from around 8 to around 12 for this angle of attack.

D. Effect of Excitation Frequency

Extensive experiments[26] have shown that excitation frequency has a strong effect on thrust and lift. Figure 12 shows the variation of the magnitude of time-averaged velocity as a function of Strouhal number for $Re = 10^4$, $\alpha = 5$ deg, and $C_\mu = 0.300$. The case of no blowing ($Sr = 0$) is included for reference. For this value of the momentum coefficient ($C_\mu = 0.300$), a time-averaged jet and positive thrust are produced for all Strouhal numbers in Fig. 12. Also, there is no separation region above the airfoil near the trailing edge; hence, complete reattachment of the flow occurs at the trailing edge. For the lowest Strouhal number $Sr = 2.9$, the time-averaged jet is broader in comparison to jets of higher excitation frequency. Also,

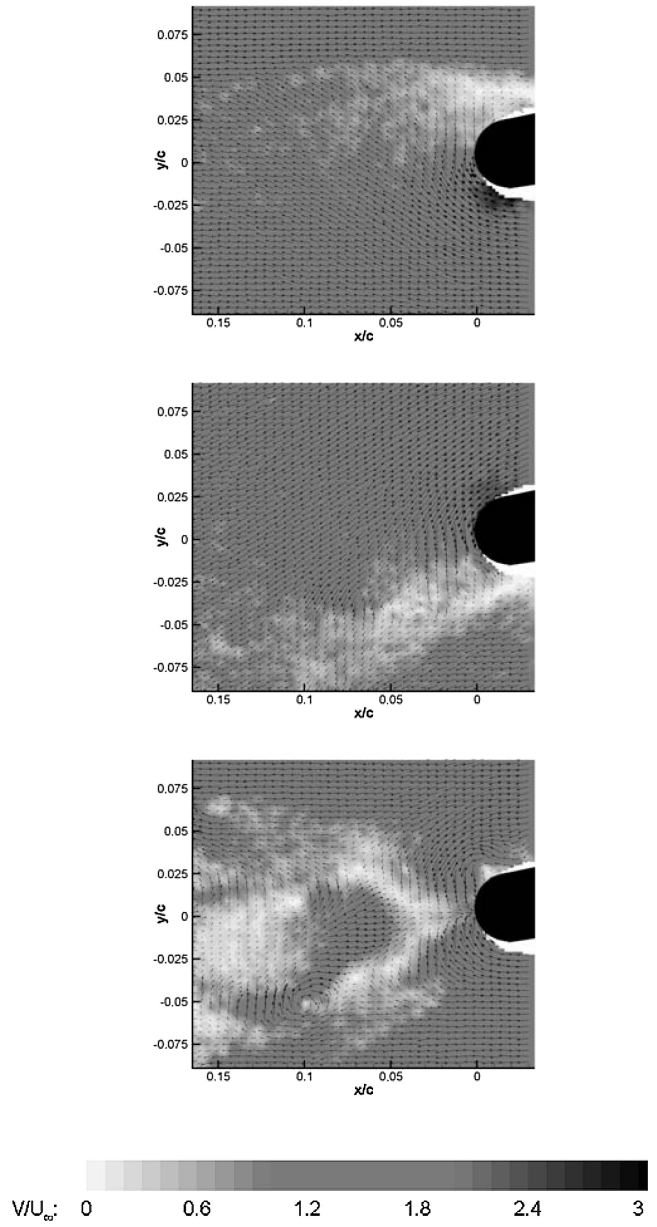

Fig. 17 Magnitude of velocity at three randomly chosen images all captured at phase h in the cycle: $Sr = 0.7$, $Re = 2 \times 10^4$, $\alpha = 5$ deg, and $C_\mu = 0.29$.

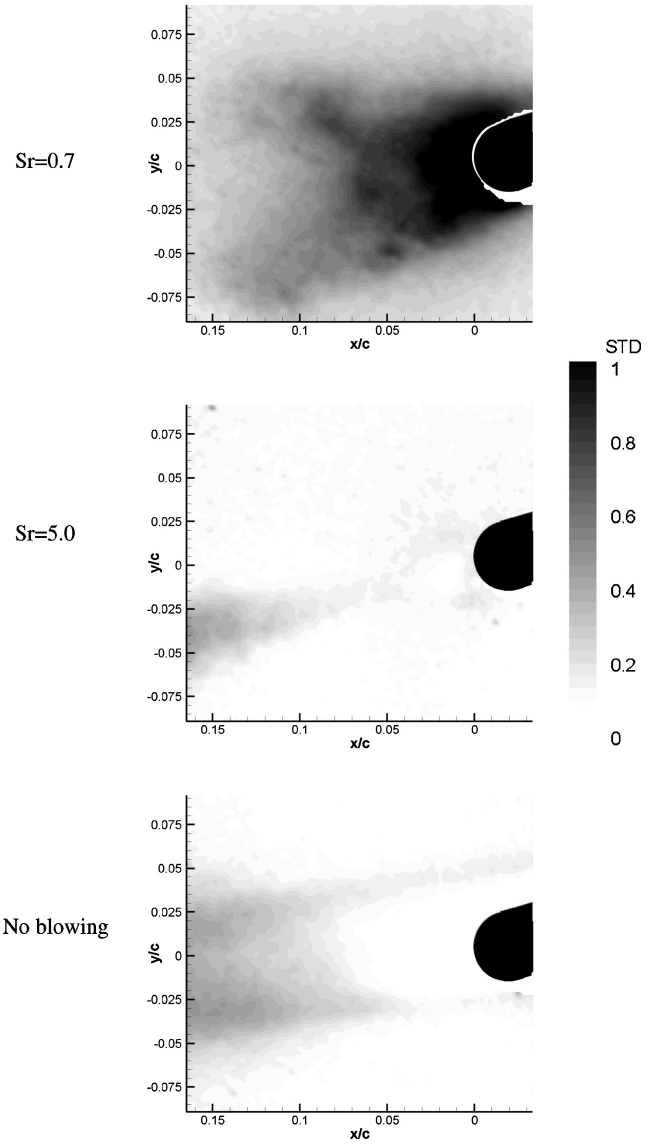

Fig. 18 Standard deviation at phase h in the cycle for $Sr = 0.7$, $Sr = 5.0$ ($C_\mu = 0.29$), and no blowing: $Re = 2 \times 10^4$, and $\alpha = 5$ deg.

with increasing Strouhal number the jets deflect slightly downward. In addition, for high Strouhal numbers the time-averaged jets are bounded above and below by lower velocity regions. The low velocity region above the jet is more pronounced, which is believed to be caused by larger entrainment.

The effect of pulse frequency is best illustrated with the time-averaged velocity profiles obtained from the LDV measurements (which provides better temporal and spatial resolution) in the wake as shown in Fig. 13. Here the Reynolds number is increased to $Re = 2 \times 10^4$, whereas the momentum coefficient is nearly the same for the same angle of attack $\alpha = 5$ deg. It is seen that jet width, as well as magnitude and location of the maximum streamwise velocity, depends on the excitation frequency. For all three Strouhal numbers, the velocity profiles suggest positive thrust, but the velocity excess and thrust appears to be maximum for the intermediate value of Strouhal number ($Sr = 5.0$). There is also some asymmetry in the velocity profile for the lowest Strouhal number $Sr = 0.7$. Only three frequencies are shown in Fig. 13 for clarity, although the data are available for a much wider range of Strouhal numbers ($Sr = 0.7$–17.1).

From the velocity profiles in the wake, the thrust coefficient can be estimated using the momentum integral technique. The net momentum flux calculated at a downstream station in the wake has often been used in unsteady flows to estimate thrust (for example, see Ref. 29); however, its limitations caused by large velocity fluctuations and deviation of pressure from the freestream value at the measurement station have been pointed out.[30,31] Nevertheless, the net momentum flux downstream defined as

$$C_M = \frac{\rho \int_{-\infty}^{\infty} u(u - U_\infty)\,\mathrm{d}y}{\frac{1}{2}\rho U_\infty^2 c}$$

provides useful information, and its variation with Strouhal number is shown in Fig. 14 for two values of momentum coefficient. It is seen that there is considerable effect of jet excitation frequency, which is more pronounced at the higher frequencies.

The momentum flux for high frequencies decreases rapidly. To understand this effect, experiments were also carried out for zero freestream velocity, that is, for the synthetic jet discharging into the fluid at rest.[11] It was found that the momentum flux decreases monotonically with increasing frequency in the same range of Strouhal numbers tested ($Sr = 0.7$–17.1). If the synthetic jet is modeled as a train of counter-rotating vortex pairs,[32,33] it can be shown that the circulation of each vortex scales with f^{-1} for a slug-like orifice exit

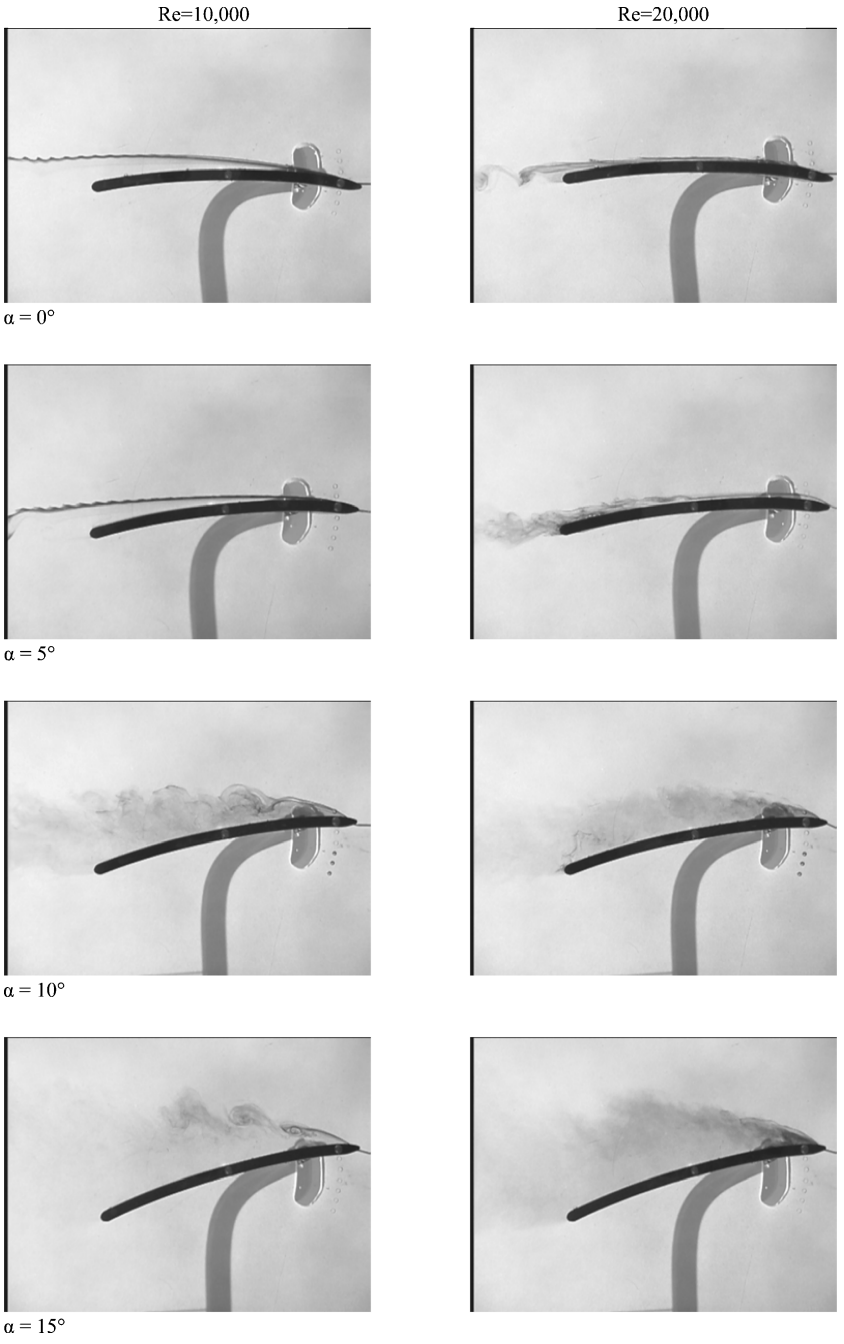

Fig. 19 Flow visualization showing the effects of Reynolds number and incidence on the airfoil without jet excitation.

velocity. Because the induced velocity is proportional to circulation, the thrust coefficient should vary as f^{-2} in this idealized case; hence, this is qualitatively similar to the experimental observations for $U_\infty = 0$. However, in the presence of a freestream, optimum frequencies in the range of $Sr = 3$–5 were observed as a result of the interaction of the synthetic jet with the separated flow over the wing.

Phase-averaged PIV measurements were taken for three different frequencies to understand the optimum frequency feature. These three frequencies correspond to the near optimum frequency ($Sr = 5.0$), lower frequency ($Sr = 0.7$), and higher frequency ($Sr = 10.0$); these are also the same frequencies shown in Fig. 13. Figure 15 shows the variation of phase-averaged vorticity at different phases in the cycle. It is seen that, for all three Strouhal numbers, reattached flow is observed during the blowing part of the cycle, that is, phases b, c, d, and e in the figure, as the vorticity over the upper surface remains close to the surface. For the optimum case ($Sr = 5.0$), the location of the vortex pair is around 0.1c at the instant of maximum blowing velocity at the orifice (phase c), whereas for the lowest frequency $Sr = 0.7$, the vortex roll-up moves out of the area of interest by the time phase b is reached. During the suction part of the cycle (phases f, g, and h in the figure), the vorticity over the upper surface still remains close to the surface for $Sr = 5.0$ and 10.0, but moves away for $Sr = 0.7$, in particular in phases g and h, which indicates flow separation.

Figure 16 shows the magnitude of the phase-averaged velocity at selected phases in the cycle. The case of no blowing is also shown for comparison. When the exit velocity at the orifice is maximum, that is, phase c, the reattachment of the flow near the trailing edge is evident for all three Strouhal numbers. However, during suction, the velocity defect grows downstream of the trailing edge for $Sr = 0.7$, and a totally separated region is observed for phase h. By contrast, for $Sr = 5.0$ and 10.0, the flow remains attached during the suction part of the cycle, even though a low-velocity region develops just downstream of the trailing edge.

Hence, it is concluded that the inability to maintain attached flow during suction for the lowest Strouhal number increases instantaneous drag and reduces the time-averaged thrust, even though the thrust of the synthetic jet alone in the fluid at rest is higher.[11] In fact, for this Strouhal number ($Sr = 0.7$) the flow is highly unsteady near the trailing edge with typical characteristics of totally separated flows. Figure 17 shows three examples of velocity fields all captured at phase h in the cycle for $Sr = 0.7$. The flowfield at the top is similar to the phase-averaged one shown in Fig. 16 and is observed most of the time. However, the two other flowfields are also possible at this phase (corresponding to the maximum suction), indicating flapping of the separated region in the vertical direction and also large occasional streamwise fluctuations caused by intermittent and symmetric suction (bottom example). This highly unsteady flow during suction for $Sr = 0.7$ is also evident from the standard deviation from the phase-averaged velocity shown in Fig. 18. In contrast, the standard deviation is negligibly small at the same phase h for $Sr = 5.0$, which indicates highly periodic and repeatable flow during suction. The case of no blowing is also shown in Fig. 18 for comparison. It is seen that low-Strouhal-number excitation results in highly unsteady flow in the wake, which is even more unsteady than for the no-blowing case. Because the massive separation regions and flapping motion are not observed during suction for $Sr = 5.0$, there is the additional benefit of operating around the optimum frequency range in addition to the maximum time-averaged thrust produced.

It was shown in Ref. 26 that the range of optimum frequency is close to the natural shedding frequency (around $Sr = 4$) in the wake with no excitation. The authors believe that this does not necessarily indicate a resonance with the global wake instability, as the flow is a lot more like a strong jet rather than a wake when forced at high momentum coefficients. This convectively unstable jet flow is driven by the excitation and does not show any resonance when the integrated energy across a downstream station is examined.[26]

E. Effect of Reynolds Number

Experiments were conducted for $Re = 10^4$ to 2×10^5 to investigate the Reynolds-number effect. This effect is most noticeable around the lowest Reynolds numbers. Figure 19 shows flow visualization for $Re = 10^4$ and 2×10^4 for various angles of attack with no blowing. It is seen that, for low angles of attack ($\alpha = 0$ and 5 deg), the flow becomes partially attached when the Reynolds number is increased to $Re = 2 \times 10^4$ even in the absence of blowing. Hence, synthetic jet blowing to overcome the drag or to produce positive thrust should be more difficult at low Reynolds numbers. The aerodynamic efficiency A_E also decreases with decreasing Reynolds number as shown in Fig. 11 and discussed earlier. Conversely, for larger incidences ($\alpha = 10$ and 15 deg), the effect of the Reynolds number is negligible.

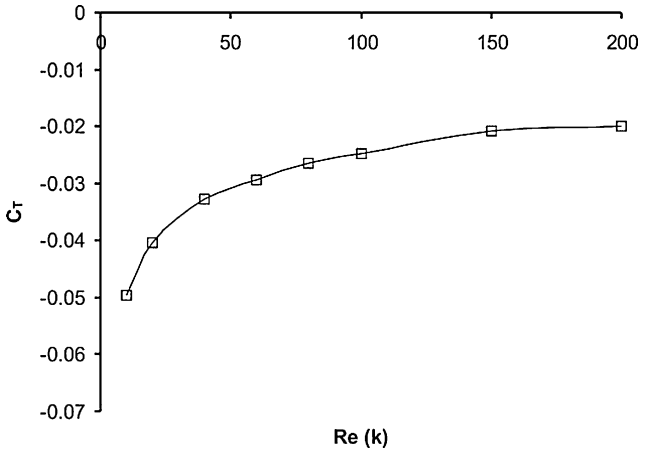

Fig. 20 Variation of estimated drag with Reynolds number without jet excitation at $\alpha = 5$ deg.

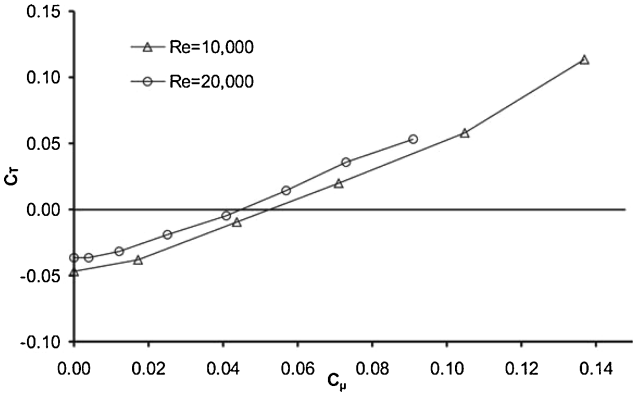

Fig. 21 Variation of estimated thrust coefficient with C_μ for two Reynolds numbers at $\alpha = 5$ deg, $Sr = 5.7$.

Figure 20 shows the variation of estimated drag coefficient for no blowing at $\alpha = 5$. It is seen that the effect of the Reynolds number is largest at the lowest Reynolds number. Figure 21 shows the variation of estimated thrust coefficient with momentum coefficient for $Re = 10^4$ and 2×10^4, at $\alpha = 5$ deg, and $Sr = 5.7$. It is seen that the thrust coefficient is larger for $Re = 2 \times 10^4$ at a given momentum coefficient. Hence, the thrust generation becomes easier. However, for a given MAV, increasing Reynolds number means increasing freestream velocity and a likely increase of thrust force and power, even though the thrust coefficient decreases. As power is a key consideration for MAVs, flight at higher Reynolds numbers might not be practically possible.

Although MAVs initially were considered to be less than 15 cm in size and therefore mostly used low-aspect-ratio wings, this restriction does not seem to be valid anymore. This work reported here is the natural starting point, and there are several high-aspect-ratio small-scale unmanned air vehicles for which this study might prove more directly relevant. Even for high-aspect-ratio wings, separated flows and large drag are typical at low Reynolds numbers. The present method is shown to be promising in this case. For low-aspect-ratio MAVs, where three-dimensional effects are dominant,[34] it remains to be seen whether the present method can be used for drag reduction and propulsion.

IV. Conclusions

The use of synthetic jets for propulsion of fixed-wing MAVs was investigated experimentally. As a thick trailing edge does not have an adverse effect on lift generation at low Reynolds numbers, a synthetic jet was placed at the trailing edge of the airfoil. Interaction of the synthetic jet with the airfoil aerodynamics was investigated with flow visualization, velocity, and pressure measurements at low Reynolds numbers. The effects of excitation frequency, momentum coefficient, angle of attack, and Reynolds number were studied in detail.

The separated region in the wake becomes smaller as the momentum coefficient is increased gradually. Once the momentum coefficient reaches a critical value, there is net zero drag. There is reattachment of the separated shear layer near the trailing edge, which causes enhancement of lift. Above the critical value of the momentum coefficient, the jet produces positive thrust. At the highest angle of attack tested ($\alpha = 15$ deg), positive thrust is not achieved for the largest momentum coefficient used. For high momentum coefficients, a region of slow flow is visible at a distance from the jet axis. The aerodynamic efficiency was investigated as a function of momentum coefficient for various angles of attack and Reynolds numbers. There is a slight decrease in the efficiency with blowing at low angles of attack, whereas this effect is negligible for higher incidences.

A strong effect of pulsing frequency has been observed, and the results suggest an optimum range of Strouhal numbers $Sr = 3$–5. The monotonous decrease of thrust coefficient with Strouhal number at zero freestream velocity is altered when the synthetic jet interacts

with the separated flow over the wing, leading to a range of optimum frequencies. Phase-averaged PIV measurements showed that attached flow during the suction part of the cycle cannot be maintained for low Strouhal numbers, and this increases the instantaneous drag and reduces the time-averaged thrust.

The separated region and drag are largest for the lowest Reynolds number in the range of Reynolds numbers tested ($Re = 10^4$ to 2×10^5). Hence relatively larger momentum coefficients are needed for $Re = 10^4$. With increasing Reynolds numbers, there is delay in the separation on the upper surface, which results in smaller separated region and drag. Hence, the reattachment of the separated shear layer is easier for higher Reynolds numbers. The favorable effect of increasing the Reynolds number is most apparent at low Reynolds numbers. It was shown that, with synthetic jet blowing, the aerodynamic efficiency improves with increasing Reynolds numbers.

Acknowledgments

This work is jointly funded by the Engineering and Physical Sciences Research Council (Grant GR/R07738/01) and the Ministry of Defence in the United Kingdom.

References

[1]Mueller, T. J., and DeLaurier, J. D., "Aerodynamics of Small Vehicles," *Annual Review of Fluid Mechanics*, Vol. 35, 2003, pp. 89–111.

[2]Shyy, W., Berg, M., and Ljungqvist, D., "Flapping and Flexible Wings for Biological and Micro Air Vehicles," *Progress in Aerospace Sciences*, Vol. 35, No. 5, 1999, pp. 455–505.

[3]Ho, S., Nassef, H., Pornsinsirirak, N. n., Tai, Y. C., and Ho, C. M., "Unsteady Aerodynamics and Flow Control for Flapping Wing Flyers," *Progress in Aerospace Sciences*, Vol. 39, No. 8, 2003, pp. 635–681.

[4]Woods, M. I., Henderson, J. F., and Lock, G. D., "Energy Requirements for the Flight of Micro Air Vehicles," *Aeronautical Journal*, Vol. 105, No. 1045, 2001, pp. 135–149.

[5]Carmichael, B. H., "Low Reynolds Number Airfoil Survey," NASA CR 165803, Vol. 1, 1981.

[6]Laitone, E. V., "Aerodynamic Lift at Reynolds Numbers Below 7×10^4," *AIAA Journal*, Vol. 34, No. 9, 1996, pp. 1941–1942.

[7]Mueller, T. J., "Aerodynamic Measurements at Low Reynolds Numbers for Fixed Wing Micro-Air Vehicles," RTO AVT/VKI, Special Course on Development and Operation of UAVs for Military and Civil Applications, von Kármán Inst., Sept. 1999.

[8]Sunada, S., Yasuda, T., Yasuda, K., and Kawachi, K., "Comparison of Wing Characteristics at an Ultralow Reynolds Number," *Journal of Aircraft*, Vol. 39, No. 2, 2002, pp. 331–338.

[9]Laitone, E. V., "Wind Tunnel Tests of Wings at Reynolds Numbers Below 70000," *Experiments in Fluids*, Vol. 23, No. 15, 1997, pp. 405–409.

[10]Whitehead, J., and Gursul, I., "Aerodynamics and Propulsion of Synthetic Jet Based Micro Air Vehicles," AIAA Paper 2003-4004, June 2003.

[11]Whitehead, J., and Gursul, I., "Interaction of Synthetic Jet Propulsion with Wing Aerodynamics at Low Reynolds Numbers," AIAA Paper 2004-0093, Jan. 2004.

[12]Ingard, U., and Labate, S., "Acoustic Circulation Effects and the Nonlinear Impedance of Orifices," *Journal of the Acoustical Society of America*, Vol. 22, No. 2, 1950, pp. 211–218.

[13]Seifert, A., and Pack, L. G., "Oscillatory Control of Separation at High Reynolds Numbers," *AIAA Journal*, Vol. 37, No. 9, 1999, pp. 1062–1071.

[14]Hsiao, F. B., Liu, C. F., and Shyu, J. Y., "Control of Wall-Separated Flow by Internal Acoustic Excitation," *AIAA Journal*, Vol. 28, No. 8, 1990, pp. 1440–1446.

[15]Williams, D., Acharya, M., Bernhadt, J., and Yang, P., "The Mechanism of Flow Control on a Cylinder with the Unsteady Bleed Technique," AIAA Paper 91-39, Jan. 1991.

[16]Williams, D., and Papazian, H., "Forebody Vortex Control with the Unsteady Bleed Technique," *AIAA Journal*, Vol. 29, No. 5, 1991, pp. 853–855.

[17]Smith, B. L., and Glezer, A., "The Formation and Evolution of Synthetic Jets," *Physics of Fluids*, Vol. 10, No. 9, 1998, pp. 2281–2297.

[18]Smith, B. L., and Glezer, A., "Vectoring and Small-Scale Motions Effected in Free Shear Flows Using Synthetic Jet Actuators," AIAA Paper 97-213, Jan. 1997.

[19]Roos, F., "Synthetic Jet Microblowing for Vortex Asymmetry Management on a Hemi-Sphere-Cylinder Forebody," AIAA Paper 97-1973, June–July 1997.

[20]Smith, D. R., Amitay, M., Kibens, V., Parekh, D., and Glezer, A., "Modification of Lifting Body Aerodynamics Using Synthetic Jet Actuators," AIAA Paper 98-209, Jan. 1998.

[21]Rizzeta, D. P., Visbal, M. R., and Stanek, M. J., "Numerical Investigation of Synthetic Jet-Flowfields," *AIAA Journal*, Vol. 37, No. 8, 1999, pp. 919–927.

[22]McCormick, D. C., "Boundary Layer Separation Control with Directed Synthetic Jets," AIAA Paper 2000-0519, Jan. 2000.

[23]Amitay, M., Smith, D. R., Kibens, V., Parekh, D. E., and Glezer, A., "Aerodynamic Flow Control over an Unconventional Airfoil Using Synthetic Jet Actuators," *AIAA Journal*, Vol. 39, No. 3, 2001, pp. 361–370.

[24]Gallas, Q., Holman, R., Nishida, T., Carroll, B., Sheplak, M., and Cattafesta, L., "Lumped Element Modeling of Piezoelectric-Driven Synthetic Jet Actuators," *AIAA Journal*, Vol. 41, No. 2, 2003, pp. 240–247.

[25]Pelletier, A., and Mueller, T. J., "Low Reynolds Number Aerodynamics of Low-Aspect-Ratio, Thin/Flat/Cambered-Plate Wings," *Journal of Aircraft*, Vol. 37, No. 5, 2000, pp. 825–832.

[26]Whitehead, J., "Aerodynamics and Propulsion of Synthetic Jet Based Micro Air Vehicles," Ph.D. Dissertation, Dept. of Mechanical Engineering, Univ. of Bath, Bath, England, U.K., Dec. 2004.

[27]Lee, C. Y., and Goldstein, D. B., "Two-Dimensional Synthetic Jet Simulation," *AIAA Journal*, Vol. 40, No. 3, 2002, pp. 510–516.

[28]Seifert, A., Eliahu, S., Greenblatt, D., and Wygnanski, I., "Use of Piezoelectric Actuators for Airfoil Separation Control," *AIAA Journal*, Vol. 36, No. 8, 1998, pp. 1535–1537.

[29]Koochesfahani, M. M., "Vortical Patterns in the Wake of an Oscillating Airfoil," *AIAA Journal*, Vol. 27, No. 9, 1989, pp. 1200–1205.

[30]Ramamurti, R., and Sandberg, W., "Simulation of Flow About Flapping Airfoils Using Finite Element Incompressible Flow Solver," *AIAA Journal*, Vol. 39, No. 2, 2001, pp. 253–260.

[31]Heathcote, S., Martin, D., and Gursul, I., "Flexible Flapping Airfoil Propulsion at Zero Freestream Velocity," *AIAA Journal*, Vol. 42, No. 11, 2004, pp. 2196–2204.

[32]Smith, B. L., and Swift, G. W., "Synthetic Jets at Large Reynolds Number and Comparison to Continuous Jets," AIAA Paper 2001-3030, March 2001.

[33]Holman, R., Utturkar, Y., Mittal, R., Smith, B. L., and Cattafesta, L., "Formation Criterion for Synthetic Jets," *AIAA Journal*, Vol. 43, No. 10, 2005, pp. 2110–2116.

[34]Gursul, I., "Vortex Flows on UAVs: Issues and Challenges," *Aeronautical Journal*, Vol. 108, No. 1090, 2004, pp. 597–610.

K. Fujii
Associate Editor